Non-yrast positive-parity structures in the γ-soft nucleus ^{156}Er

J. M. Rees, E. S. Paul, M. A. Riley, J. Simpson, A. D. Ayangeakaa, H. C. Boston, M. P. Carpenter, C. J. Chiara, U. Garg, D. J. Hartley, R. V. F. Janssens, D. S. Judson, F. G. Kondev, T. Lauritsen, N. M. Lumley, J. Matta, P. J. Nolan, J. Ollier, M. Petri, J. P. Revill, L. L. Riedinger, S. V. Rigby, C. Unsworth, X. Wang, and S. Zhu

Phys. Rev. C **83**, 044314 — Published 22 April 2011

DOI: 10.1103/PhysRevC.83.044314

Non-yrast positive-parity structures in the gamma-soft nucleus ^{156}Er

J. M. Rees,[1] E. S. Paul,[1,*] M. A. Riley,[2] J. Simpson,[3] A. D. Ayangeakaa,[4] H. C. Boston,[1] M. P. Carpenter,[5] C. J. Chiara,[5,6] U. Garg,[4] D. J. Hartley,[7] R. V. F. Janssens,[5] D. S. Judson,[1] F. G. Kondev,[8] T. Lauritsen,[5] N. M. Lumley,[9] J. Matta,[4] P. J. Nolan,[1] J. Ollier,[3] M. Petri,[10] J. P. Revill,[1] L. L. Riedinger,[11] S. V. Rigby,[1] C. Unsworth,[1] X. Wang,[2] and S. Zhu[5]

[1]*Oliver Lodge Laboratory, University of Liverpool, Liverpool L69 7ZE, United Kingdom*
[2]*Department of Physics, Florida State University, Tallahassee, Florida 32306, U.S.A.*
[3]*STFC Daresbury Laboratory, Daresbury, Warrington WA4 4AD, United Kingdom*
[4]*Physics Department, University of Notre Dame, Notre Dame, Indiana 46556, U.S.A.*
[5]*Physics Division, Argonne National Laboratory, Argonne, Illinois 60439, U.S.A.*
[6]*Department of Chemistry and Biochemistry, University of Maryland, College Park, Maryland 20742, U.S.A.*
[7]*Department of Physics, United States Naval Academy, Annapolis, Maryland 21402, U.S.A.*
[8]*Nuclear Engineering Division, Argonne National Laboratory, Argonne, Illinois 60439, U.S.A.*
[9]*Schuster Laboratory, University of Manchester, Manchester M13 9PL, United Kingdom*
[10]*Nuclear Science Division, Lawrence Berkeley National Laboratory, Berkeley, California 94720, U.S.A.*
[11]*Department of Physics and Astronomy, University of Tennessee, Knoxville, Tennessee 37996, U.S.A.*

Weakly populated band structures have been established in ^{156}Er at low to medium spins, following the ^{114}Cd(^{48}Ca,6nγ) reaction at 215 MeV. High-fold γ-ray coincidence data were recorded in a high-statistics experiment with the Gammasphere spectrometer. Bands built on the second 0^+ and 2^+ (γ-vibrational) states have been established. A large energy staggering between the even- and odd-spin members of the γ-vibrational band suggests a γ-soft nature of this nucleus. An additional band is discussed as being based on a rotationally aligned $(\nu h_{9/2}, f_{7/2})^2$ structure, coexisting with the systematically observed, more favorable $(\nu i_{13/2})^2$ aligned structure seen in this mass region.

PACS numbers: 27.70.+q, 21.10.Re, 23.20.Lv, 23.20.En

I. INTRODUCTION

The way in which the atomic nucleus generates excited states and increasing angular momentum represents a delicate interplay between single-particle and collective degrees of freedom. The addition of valence nucleons to spherical, closed-core nuclei breaks the spatial symmetry, allowing rotation of the now deformed system to compete energetically with single-particle and vibrational modes of excitation. The nuclide $^{156}_{68}$Er$_{88}$, with only ten valence particles outside the ^{146}Gd doubly magic core, lies in a 'transitional' region where nuclear collectivity rapidly changes from vibrational to rotational motion [1]. This is reflected in a sharp change in the experimental $E(4^+)/E(2^+)$ energy ratios between $N = 86$ and $N = 96$ nuclei for isotopes with Z around 64, as shown in Fig. 1. $E(4^+)/E(2^+)$ ratios of 2.00 and 3.33 are expected for pure vibrational and rotational behavior, respectively. For the erbium isotopes ($Z = 68$), ^{154}Er has an $E(4^+)/E(2^+)$ ratio that lies close to the vibrational limit, while ^{160}Er, with only six more valence neutrons, already lies close to the rotational limit. The intermediate ^{156}Er isotope has an $E(4^+)/E(2^+)$ ratio approaching 2.50, the value expected for a γ-soft rotor [2], where vibrational modes of excitation couple to rotation [3].

The primary aim of the present experiment was to measure quadrupole moments of ultrahigh-spin collective bands in ^{157,158}Er [4, 5], using the Doppler Shift Attenuation Method [6]. Significant new information has also been found in $^{156}_{68}$Er$_{88}$ at low spin with the observation of weakly populated non-yrast structures. In particular, a band built on an excited 0^+ state has been established to $(22\hbar)$, while both even- and odd-spin members of the γ-vibrational band have been identified to $\sim 15\hbar$. The relative energies of the even- and odd-spin states of the

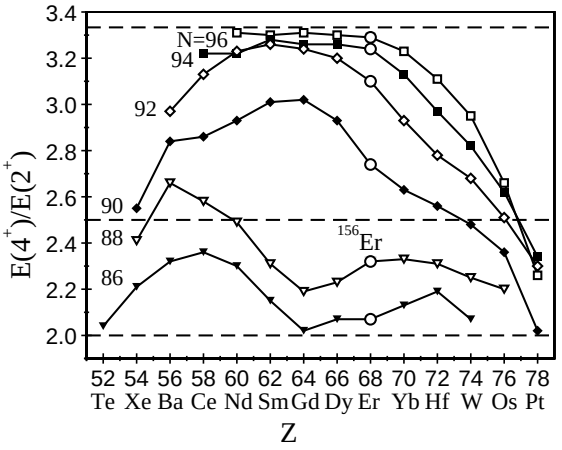

FIG. 1: $E(4^+)/E(2^+)$ energy-ratio systematics for even-even nuclei as a function of atomic number Z. The Er isotopes are denoted by open circles. The horizontal dashed lines represent limits expected for pure vibrational (2.00), rotational (3.33), and γ-soft (2.50) behavior, respectively.

*Corresponding author: esp@ns.ph.liv.ac.uk

γ-vibrational band determine the nature of triaxiality in this nucleus [7], i.e. whether it is γ rigid or γ soft. These new low-spin, non-yrast structures complement a comprehensive high-spin study of ^{156}Er [8]; both experiments were performed using the highly efficient Gammasphere spectrometer [9, 10]. The new structures in ^{156}Er are compared with those in neighboring isotones ($N = 88$) and isotopes ($Z = 68$).

II. EXPERIMENTAL DETAILS AND RESULTS

The nucleus ^{156}Er was studied at Argonne National Laboratory, using the Gammasphere spectrometer equipped with 101 HPGe detectors. A ^{48}Ca beam of energy 215 MeV was delivered by the ATLAS facility and used to bombard a 1-mg/cm^2 ^{114}Cd target, backed by a 13-mg/cm^2 layer of ^{197}Au, to produce ^{156}Er via the 6n evaporation channel. An additional 0.07-mg/cm^2 layer of ^{27}Al between the Cd and Au was used to prevent the migration of the target material into the backing. The use of the backed target maintained full intrinsic γ-ray energy resolution, particularly at low spin, since the vast majority of transitions were emitted after the recoiling nuclei had already stopped and hence were not susceptible to Doppler broadening of the line shapes.

A total of approximately 10^{10} events was accumulated over 12 days of beam time when at least four Compton-suppressed HPGe detectors fired in prompt time coincidence. In the off-line analysis, approximately 10^{11} quadruple-coincident events (γ^4) were unfolded from the raw data and replayed into a Radware-format four-dimensional hypercube [11, 12] for subsequent analysis. The three most strongly populated nuclei, ^{156}Er (6n), ^{157}Er (5n), and ^{158}Er (4n), were observed in the hypercube at an approximate ratio of 0.5:1.0:1.0.

A. New non-yrast levels in ^{156}Er

The low-lying levels in ^{156}Er, deduced from this work, are shown in Fig. 2. The band-numbering convention is adopted from Ref. [8]. Four weakly populated band structures, labeled 2, 7, 8, and 9, have been established in ^{156}Er with maximum intensities around 0.5% of the 344 keV $2^+ \rightarrow 0^+$ transition. Previously, states up to 4^+ were seen in Bands 2 and 7 from studies of the radioactive decay of ^{156}Tm; in addition, the 3^+ level of Band 8 was identified [13, 14], although subsequent work reassigned this level to 4^+ [15]. Band 2 has been extended to $I^\pi = 14^+$ and Band 7 to $I^\pi = (22^+)$. Both of these bands decay into Band 1, the ground-state band, via a series of $\Delta I = 2$ and $\Delta I = 0$ transitions. The levels of Band 9 are newly identified in the present study. The coincident γ-ray spectra of Fig. 3 show the new transitions in Bands 8 and 9, respectively.

B. Spin and parity assignments

To assist in assigning spins and parities to transitions in the level scheme, γ-ray multipolarities were extracted from the data by conducting an angular-correlation analysis using the method of directional correlation from oriented states (DCO) [16]. An angular-intensity ratio,

$$R = \frac{I_{\gamma\gamma}[\theta \approx 130^\circ(50^\circ)]}{I_{\gamma\gamma}[\theta \approx 90^\circ]}, \quad (1)$$

was evaluated for many of the new γ-ray transitions. Typical angular-intensity ratios extracted from this analysis were $\sim$0.7 for a pure stretched dipole ($\Delta I = 1$) transition, and $\sim$1.1 for a stretched quadrupole ($\Delta I = 2$) transition. Results for the transitions assigned to ^{156}Er reported in this work are listed in Table I.

TABLE I: Angular-intensity ratios and spin/parity assignments for transitions in Bands 2, 2a, 7, 8 and 9. Results are also included for some known strong $E2$ and $E1$ transitions in ^{156}Er.

E_γ (keV) [a]	R	Assignment
known $E2$ transitions		
344.2	1.11(5)	$2^+ \rightarrow 0^+$
452.4	1.30(6)	$4^+ \rightarrow 2^+$
543.1	1.16(6)	$6^+ \rightarrow 4^+$
617.9	1.17(9)	$8^+ \rightarrow 6^+$
674.1	0.98(19)	$10^+ \rightarrow 8^+$
known $E1$ transitions		
530.4	0.73(6)	$9^- \rightarrow 8^+$
688.6	0.64(19)	$7^- \rightarrow 6^+$
Bands 2, 2a transitions		
475.0		$4^+ \rightarrow 2^+$
479.7		$6^+ \rightarrow 4^+$
490.6		$8^+ \rightarrow 6^+$
501.6		$18^+ \rightarrow 16^+$
544.7		$6^+ \rightarrow 6^+$
555.7		$18^+ \rightarrow 16^+$
557.3		$14^+ \rightarrow 12^+$
565.8		$10^+ \rightarrow 8^+$
585.5		$2^+ \rightarrow 2^+$
596.7		$16^+ \rightarrow 14^+$
608.1		$4^+ \rightarrow 4^+$
645.2		$12^+ \rightarrow 10^+$
684.3		$12^+ \rightarrow 10^+$
692.1		$14^+ \rightarrow 12^+$
870.4		$14^+ \rightarrow 12^+$
930.4		$2^+ \rightarrow 0^+$
1036.3		$8^+ \rightarrow 6^+$
1060.0		$4^+ \rightarrow 2^+$
1088.4		$6^+ \rightarrow 4^+$

[a] The γ-ray energies are estimated to be accurate to $\pm$0.3 keV.

It has been possible to measure the angular-intensity ratios of most of the Band 7 and Band 9 transitions, together with the 1038-keV transition linking Band 8 with the ground-state band (Band 1); the results are presented

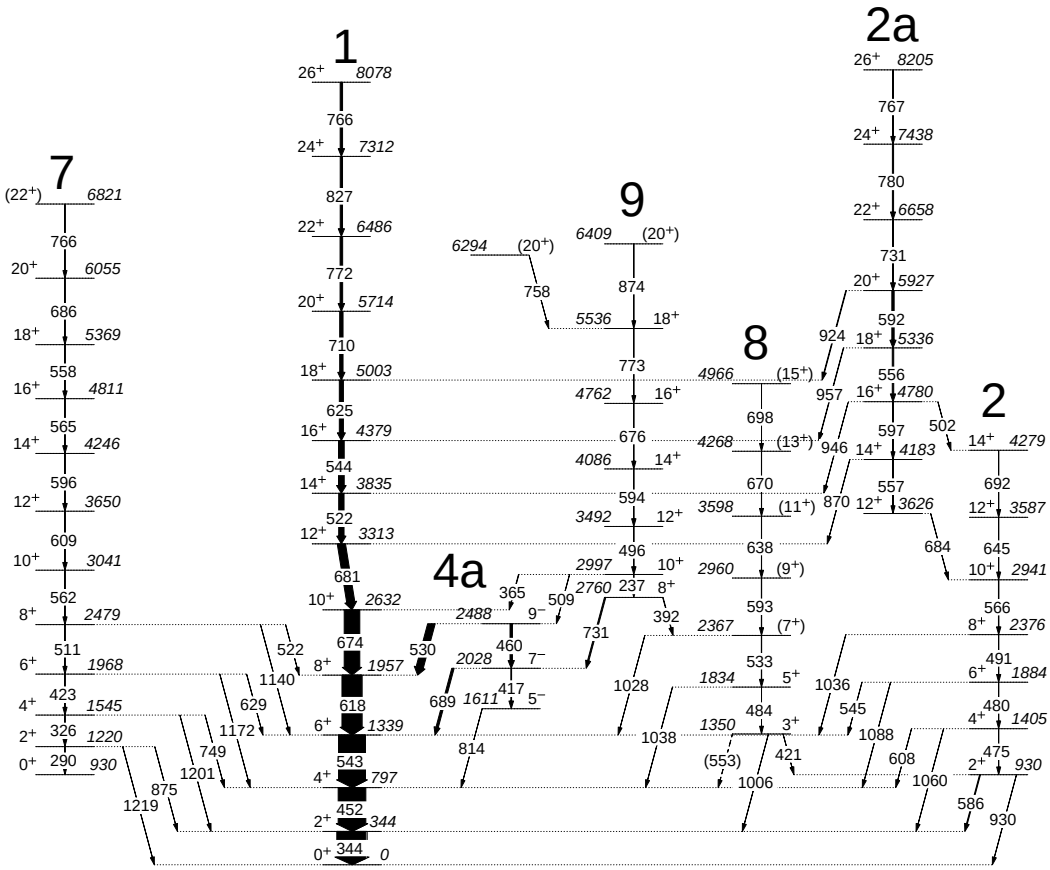

FIG. 2: Partial level scheme, up to $I = 26$, deduced for ^{156}Er from the present work and showing new Bands 2, 7, 8, and 9 in relation to known Bands 1, 2a, and 4a [8]. Energies are labeled in keV and the widths of the arrows are proportional to the transition intensities.

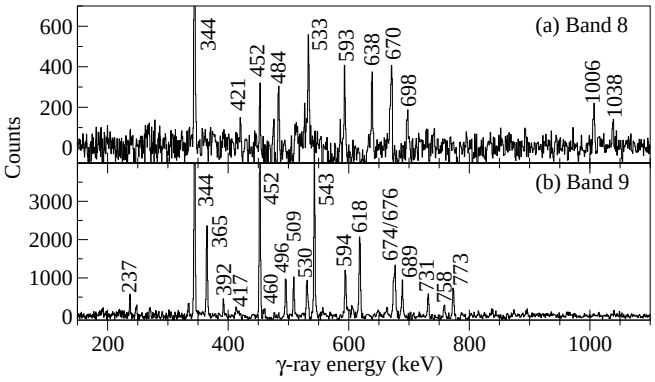

FIG. 3: Triple-gated spectra of quadruple γ-ray events showing transitions in (a) Band 8 and (b) Band 9.

in Table I. Angular-intensity ratios of established transitions have been included for reference and comparison. The 0.55 angular-intensity ratio of the 1038-keV transitions strengthens the $I = 5$ assignment of the level at 1834 keV and, by extension, the odd-spin $\alpha = 1$ signature of Band 8. The original 3^+ assignment to the level at 1350 keV [13] is therefore confirmed rather than the subsequent 4^+ reassignment [15]. This level decays to the 2^+ level of Band 2 through a 421-keV transition, to the 2^+ level of Band 1 through a 1006-keV transition, and possibly to the 4^+ level of Band 1 through a tentative 553-keV transition.

The low-energy 237-keV transition at the bottom of Band 9 has an angular-intensity ratio of 1.3, suggesting it is a stretched quadrupole transition, although a non-stretched dipole assignment cannot be ruled out. This implies that the levels at energies of 2760 and 2997 keV are separated in spin by 0 or 2. The 365-keV transition, connecting the 2997-keV level of Band 9 to the yrast 10^+ state of Band 1, has an angular-intensity ratio of 0.27. This value is much too low for a pure dipole ($E1$, $\Delta I = 0, 1$) transition, so the transition probably corresponds to an $M1/E2$ transition with a large negative mixing ratio, using the sign convention of Ref. [17]. The state at 2997 keV in Band 9 could then be assigned 9^+, 10^+, or 11^+. The latter assignment can be rejected since Band 9 would be too yrast and would have to decay to the negative-parity Band 4a through hindered stretched $M2$ transitions. The 509-keV transition, feeding into the 9^- level of Band 4a, has an angular-intensity ratio consistent with a pure stretched ($\Delta I = 1$) dipole and is hence

Table I continued.

E_γ (keV) [a]	R	Assignment
	Band 7 transitions	
289.5		$2^+ \rightarrow 0^+$
325.5		$4^+ \rightarrow 2^+$
422.9	1.18(12)	$6^+ \rightarrow 4^+$
510.9		$8^+ \rightarrow 6^+$
521.8		$8^+ \rightarrow 8^+$
557.7	1.10(13)	$18^+ \rightarrow 16^+$
561.7	1.04(9)	$10^+ \rightarrow 8^+$
565.4	1.09(6)	$16^+ \rightarrow 14^+$
596.2	1.14(11)	$14^+ \rightarrow 12^+$
608.9		$12^+ \rightarrow 10^+$
628.6	0.79(20)	$6^+ \rightarrow 6^+$
686.5	1.29(24)	$20^+ \rightarrow 18^+$
748.7	0.65(23)	$4^+ \rightarrow 4^+$
766.0		$(22^+) \rightarrow 20^+$
875.4		$2^+ \rightarrow 2^+$
1139.7		$8^+ \rightarrow 6^+$
1172.1	1.08(43)	$6^+ \rightarrow 4^+$
1201.2	0.94(26)	$4^+ \rightarrow 2^+$
1219.4		$2^+ \rightarrow 0^+$
	Band 8 transitions	
420.6		$3^+ \rightarrow 2^+$
483.7		$5^+ \rightarrow 3^+$
533.5		$(7^+) \rightarrow 5^+$
(553.4)		$3^+ \rightarrow 4^+$
592.7		$(9^+ \rightarrow 7^+)$
638.0		$(11^+ \rightarrow 9^+)$
670.5		$(13^+ \rightarrow 11^+)$
697.6		$(15^+ \rightarrow 13^+)$
1006.0		$3^+ \rightarrow 2^+$
1027.8		$(7^+) \rightarrow 6^+$
1038.0	0.55(9)	$5^+ \rightarrow 4^+$
	Band 9 transitions	
237.2	1.31(24)	$10^+ \rightarrow 8^+$
364.6	0.27(3)	$10^+ \rightarrow 10^+$
392.4		$8^+ \rightarrow (7^+)$
495.6	1.12(14)	$12^+ \rightarrow 10^+$
508.6	0.76(5)	$10^+ \rightarrow 9^-$
593.9	1.28(12)	$14^+ \rightarrow 12^+$
676.4	0.97(20)	$16^+ \rightarrow 14^+$
731.4	1.01(14)	$8^+ \rightarrow 7^-$
758.3		$(20^+) \rightarrow 18^+$
773.1	1.05(18)	$18^+ \rightarrow 16^+$
873.8		$(20^+) \rightarrow 18^+$

[a] The γ-ray energies are estimated to be accurate to ± 0.3 keV.

assigned to have $E1$ character. This fixes the 2997-keV state to have $I^\pi = 10^+$ and consequently the band-head of Band 9 to have spin and parity 8^+. The 731-keV transition which decays from the 8^+ band-head to the 7^- state of Band 4a has a high angular-intensity ratio (1.01 ± 0.14) but the large error bar means that it is not inconsistent with a stretched $E1$ assignment.

III. DISCUSSION

The rotational model [18] that couples together both collective rotations and vibrations [3] is appropriate for the description of ^{156}Er. In addition, this nucleus has been discussed [19] in the context of the interacting boson model (IBM), which is able to describe the collective properties of nuclei spanning a large variety of structures with a single Hamiltonian [20]. The $E(4^+)/E(2^+)$ ratio of 2.32 for ^{156}Er (see Fig. 1) lies above the U(5) vibrational limit of this model (2.00), but below the SU(3) rotational limit (3.33); the ratio is in fact nearer to the O(6) limit for a γ-soft rotor (2.50). The second 0^+ and 2^+ states are degenerate, at an excitation energy of 930 keV [14]. Moreover, they lie close to the yrast 4^+ energy, as expected for a U(5) vibrator. Transitional rare-earth nuclei, lying close to spherical-deformed phase transitions, required the introduction of dynamical symmetries [21, 22] to adequately describe the structural evolution of these nuclei. Such a description, using a simplified two-parameter Hamiltonian [23], has been able to reproduce the properties of low-lying positive-parity excitations in these nuclei rather well. Recent work, using the triaxial projected shell model [24], has also focused on the theoretical description of γ-vibrational bands in the light erbium isotopes where they are predicted to become close to yrast at high spin.

A. Systematics of second 0^+ states

The lowest levels of Band 7 were originally associated with a $K^\pi = 0^+$ β-vibrational band [13]. However, due to the low excitation energy of the 0^+ band-head (930 keV), such an interpretation has subsequently been questioned [25]. Other interpretations have also been proposed for low-lying excited 0^+ levels, including pairing isomers [26] and a second vacuum formed by particle-hole excitations [27–29]. Energy systematics of the first excited 0_2^+ states in $N = 88$ isotones and $Z = 68$ (erbium) isotopes [30] are shown in Fig. 4, where $E(0_2^+)/E(2_1^+)$ energy ratios are plotted; the values span a range 2–18. The lowest $E(0_2^+)/E(2_1^+)$ ratio in these particular nuclei occurs in ^{152}Gd, an isotope with a semi-magic $Z = 64$ protons. On the other hand, the largest ratio occurs in ^{166}Er with 98 neutrons.

B. Systematics of γ-vibrational states

In this work, Bands 2 and 8 are interpreted as the two signature components of the $K^\pi = 2^+$ γ-vibrational band in ^{156}Er. The low-lying γ-vibrational band energies are plotted in Fig. 5 for $N = 88$ isotones and $Z = 68$ (erbium) isotopes [30, 35, 36], together with the energies of the first 2^+ and 4^+ states and the second 0^+ states. For the $N = 88$ isotones, Fig. 5(a), the second 0^+ state lies well below the 2_γ^+ band-head, except for ^{156}Er ($Z = 68$)

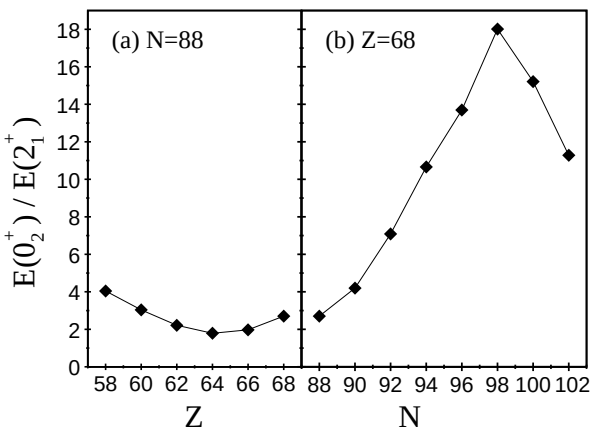

FIG. 4: Energy ratios $E(0_2^+)/E(2_1^+)$ for (a) $N = 88$ isotones and (b) $Z = 68$ isotopes.

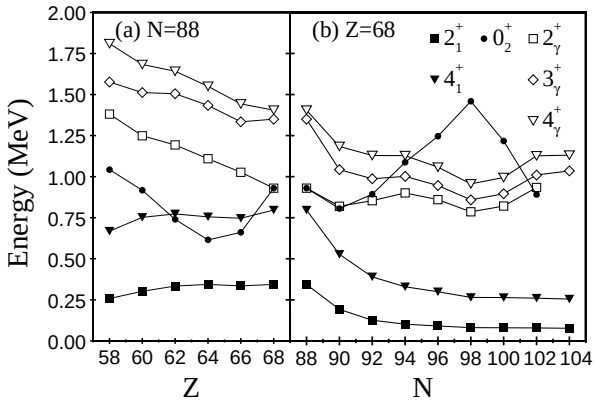

FIG. 5: Systematic energies of the lowest γ-vibrational levels and 0_2^+ states in (a) $N = 88$ isotones and (b) $Z = 68$ isotopes, relative to the nuclear ground state. The 2_1^+ and 4_1^+ levels are also included. Note that the 0_2^+ and 2_γ^+ levels are degenerate in ^{156}Er ($N = 88, Z = 68$), and also lie close to the 4_1^+ state.

where the two levels become degenerate. Moreover, the second 0^+ state also falls below the first 4^+ state for $Z = 62 - 66$ (^{150}Sm, ^{152}Gd, and ^{154}Dy). For the $Z = 68$ isotopes, Fig. 5(b), the second 0^+ state and 2_γ^+ levels remain close together for $N = 88 - 92$ (^{156,158,160}Er), before the second 0^+ state rapidly rises in energy. The second 0^+ energy peaks for $N = 98$ (^{166}Er), which also has the lowest γ-vibrational energies, before dropping for the heavier isotopes. This could indicate a change of intrinsic structure for the second 0^+ state in these heavier isotopes, e.g. an intruder configuration [23]. The second 0^+ state even falls below the 2_γ^+ level for $N = 102$ (^{170}Er), but has not been experimentally identified for $N = 104$ (^{172}Er). In ^{156}Er, the degenerate second 0^+ and 2_γ^+ states also lie close to the yrast 4^+ state, as expected for a vibrational nucleus.

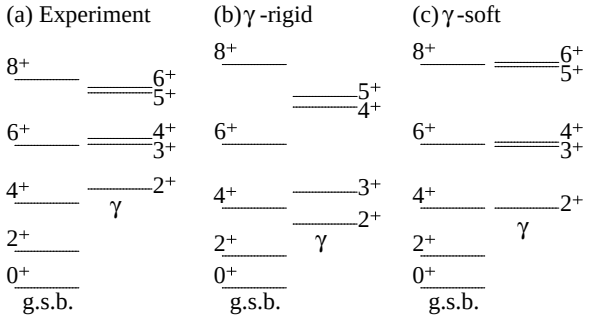

FIG. 6: Comparison of the energy of the ground-state band (g.s.b.) and energy staggering of (a) the experimental γ-band proposed in this work, with schematic staggering [7] predicted by (b) the γ-rigid asymmetric-rotor model with $\gamma = 30^\circ$ and (c) the γ-soft rotor model with $\bar{\gamma} = 30^\circ$.

C. Nature of the triaxiality

The energy staggering between the even- and odd-spin members of the γ-vibrational band can provide an insight into the nature of the nuclear triaxiality [7]. In particular, the energy staggering can distinguish between rigid and γ-soft triaxial shapes. Rigid triaxial nuclear shapes are described by the asymmetric-rotor model (ARM) of Davydov and Filippov [31], in which the potential has a well-defined minimum at a particular value of γ. The other possibility, that there is not static triaxial deformation, but instead dynamic oscillations in γ, is described in its most extreme case by the Wilets-Jean model [32]. This model considers complete γ-instability, described by a nuclear potential that has a finite favored β value, but is completely flat with respect to γ; the nucleus in effect oscillates uniformly between $\gamma = 0^\circ$ (prolate) and $\gamma = 60^\circ$ (oblate).

In the rigid triaxial case, γ-band levels appear in doublets as $(2_\gamma^+ - 3_\gamma^+)$, $(4_\gamma^+ - 5_\gamma^+)$, $(6_\gamma^+ - 7_\gamma^+)\ldots$, but the γ-soft case results in a 2_γ^+, $(3_\gamma^+ - 4_\gamma^+)$, $(5_\gamma^+ - 6_\gamma^+)\ldots$ pattern [2, 33]. The predicted level structures are shown schematically [7] in Fig. 6 for the Davydov model at $\gamma = 30^\circ$ and for the Wilets-Jean model with $\bar{\gamma} = 30^\circ$. The reduced experimental level scheme, Fig. 6(a), clearly has the energy staggering predicted by the γ-soft model. Furthermore, the experimental 3_γ^+ and 4_γ^+ levels lie close to the yrast 6^+ state, as expected for the γ-soft shape. A more quantitative approach involves measuring the energy staggering [34] of the band, defined for spin I as

$$S(I) = \frac{[E(I) - E(I-1)] - [E(I-1) - E(I-2)]}{E(2_1^+)}. \quad (2)$$

The ground-state band and γ-vibrational band energies, together with the energy staggering parameter $S(I)$, are shown up to $I = 16$ for the new levels in ^{156}Er in Fig. 7. It can be seen that the energy staggering persists up to the highest spins.

Systematics of the $S(4)$ values are shown in Fig. 8. Rotation of a γ-rigid triaxial shape with $\gamma = 0^\circ$, i.e. an axial

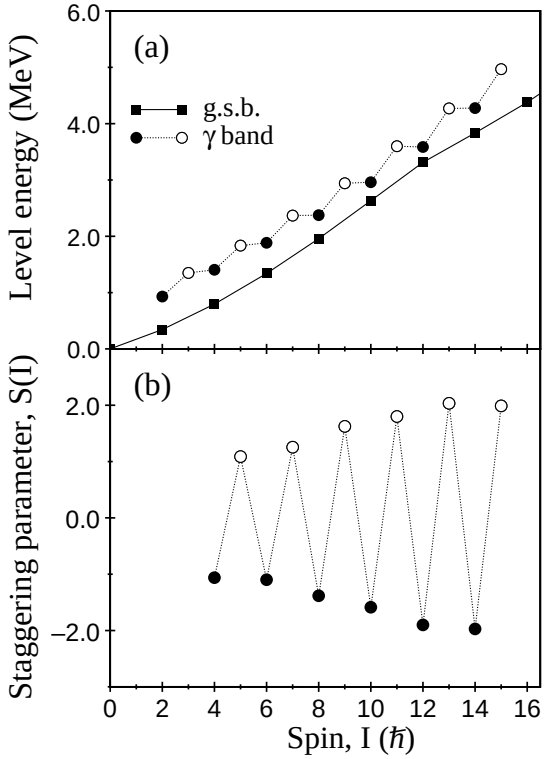

FIG. 7: (a) Level energies of the ground-state band and γ-vibrational band in ^{156}Er, plotted as a function of spin. (b) $S(I)$ values of the γ-vibrational band, plotted as a function of spin.

prolate nucleus, yields a value of $S(4) = 0.33$. However, a γ-rigid rotor with $\gamma = 30°$ is predicted to have an $S(4)$ value of +1.67 while a γ-soft rotor with $\bar{\gamma} = 30°$ has an $S(4)$ value around –1.0 [7]. A spherical vibrator should also have $S(4) = -1.0$. It can be seen in Fig. 8 that

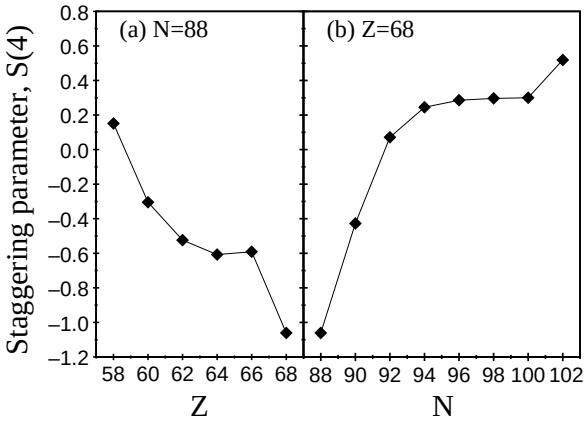

FIG. 8: Measured $S(4)$ values for (a) $N = 88$ isotones and (b) $Z = 68$ isotopes.

the $S(4)$ value for ^{156}Er is very close to –1.0, and is the lowest value amongst these particular $N = 88$ isotones and $Z = 68$ isotopes. Thus ^{156}Er is an ideal candidate

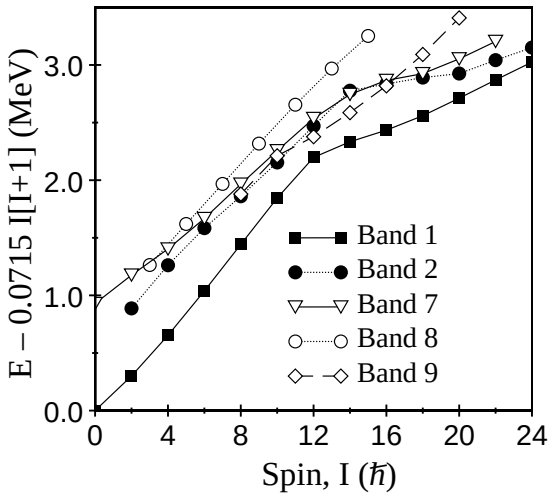

FIG. 9: Energies, relative to a rotating liquid-drop reference, of the low-spin bands in ^{156}Er, plotted as a function of spin.

for the archetypical γ-soft rotor. Furthermore, the heavier Er isotopes quickly approach the limit of $S(4) = 0.33$, expected for rigid-γ behavior. Taken with the energy systematics of Fig. 1, this shows that the Er isotopes above ^{156}Er rapidly change from rotation-vibration (γ-soft) behavior to deformed rotational (prolate) behavior. This can be explained by the neutron Fermi surface moving into the deformation-driving $\nu i_{13/2}$ sub-shell. The $S(4)$ value increases above 0.33 for ^{170}Er ($N = 102$), indicating a lowering of the odd-spin γ-vibrational band members relative to the even-spin members. Such a situation suggests the onset of (rigid) triaxiality, see Fig. 6(b). It can also be seen in Fig. 5(b) that the second 0^+ state becomes near-degenerate with the 2^+_γ band-head for this isotope.

D. Alignment properties of the bands

The energy levels of the new band structures in ^{156}Er are plotted in Fig. 9 as a function of spin, where they are compared with those of the yrast ground-state band (Band 1). A rotating liquid-drop reference has been subtracted from each structure. The changes in slopes represent rotational alignment of specific quasiparticle pairs.

In order to investigate the rotational properties of the new bands in ^{156}Er, the experimental alignments [37],

$$i_{\rm x}(\omega) = I_{\rm x}(\omega) - I_{\rm x,ref}(\omega), \qquad (3)$$

are shown in Fig. 10, plotted as a function of rotational frequency, $\omega = E_\gamma/\Delta I_x \approx E_\gamma/2\hbar$. At a given spin I, the aligned spin is $I_{\rm x} = \sqrt{I(I+1) - K^2}$, while the rotational reference, $I_{\rm x,ref}$, is given by

$$I_{\rm x,ref}(\omega) = \omega(\mathcal{J}_0 + \mathcal{J}_1\omega^2) - i_0. \qquad (4)$$

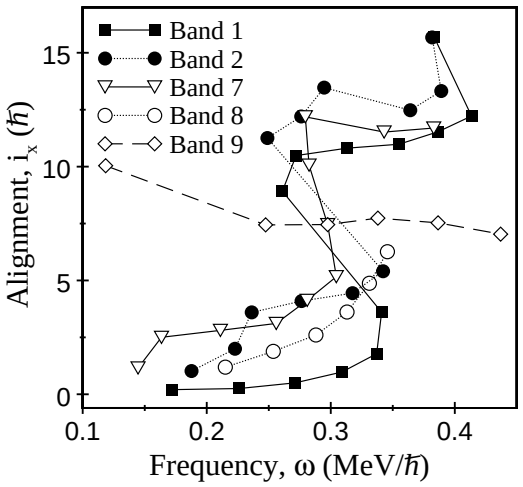

FIG. 10: Experimental alignments, i_x, as a function of rotational frequency, ω, for positive-parity bands in ^{156}Er.

Harris parameters [38, 39] $\mathcal{J}_0 = 32.1\ \hbar^2\text{MeV}^{-1}$ and $\mathcal{J}_1 = 34.0\ \hbar^4\text{MeV}^{-3}$, obtained from ^{157}Ho [40], have been used together with a positive offset $i_0 = 4.4\hbar$ in order to ensure that the ground-state band of ^{156}Er has approximately zero alignment at low rotational frequency [8]. For the γ-vibrational bands (Bands 2 and 8), $K = 2$ was used and elsewhere $K = 0$.

Band 1 gains $10 - 11\hbar$ of alignment at a rotational frequency of approximately 0.3 MeV/$\hbar$. In addition, Bands 2 and 7 show a similar alignment gain at this frequency, while Band 8 shows a more gradual upbend. This alignment gain is due to breaking a pair of $\nu i_{13/2}$ quasineutrons, as typically seen in this mass region. Hence in ^{156}Er, a rotationally aligned $(\nu i_{13/2})^2$ two-quasineutron configuration is seen coupled to three different intrinsic states, namely the 0^+ ground state, and also the 0_2^+ and 2_γ^+ states. The increase in alignment of Bands 1 and 2 at $\omega \sim 0.4$ MeV/$\hbar$ represents the onset of a shape change from prolate to oblate in ^{156}Er, culminating in band termination at $I^\pi = 42^+$, as discussed in detail in Ref. [8].

Newly identified Band 9 carries less alignment ($\sim 7.5\hbar$) than Band 1 above the rotational alignment of $i_{13/2}$ neutrons ($\omega > 0.3$ MeV/$\hbar$). This could be explained if Band 9 instead corresponds to a rotationally aligned $(\nu h_{9/2}, f_{7/2})^2$ configuration (the negative-parity $h_{9/2}$ and $f_{7/2}$ orbitals are strongly mixed). Indeed, such an aligned configuration has been proposed in the $N = 88$ ^{162}W isotone [41], while competition between $(\nu i_{13/2})^2$ and $(\nu h_{9/2}, f_{7/2})^2$ rotational alignments has recently been observed in $N = 89$ ^{163}W [42] and $N = 88$ ^{161}Ta [43].

IV. CONCLUSIONS

A high-statistics experiment with the Gammasphere spectrometer has unearthed new non-yrast structures in ^{156}Er at low spin. A band built on a low-lying second 0^+ state has been established to $I^\pi = (22^+)$. In addition, both odd- and even-spin components of the γ-vibrational band have been identified, and the energy staggering between them resembles that expected for a γ-soft rotor. Finally, a band attributed to an aligned $(\nu h_{9/2}, f_{7/2})^2$ configuration has been followed to $I^\pi = (20^+)$. With this interpretation, ^{156}Er is the first even-even nucleus, in this mass region, in which competing $(\nu h_{9/2}, f_{7/2})^2$ and $(\nu i_{13/2})^2$ alignments have been established.

Acknowledgments

The authors acknowledge Paul Morrall for preparing the targets, and the ATLAS operations staff for the beam support. This work has been supported in part by the U.S. National Science Foundation under grants No. PHY-0756474 (FSU), PHY-0554762 (USNA), and PHY-0754674 (UND), the U.S. Department of Energy, Office of Nuclear Physics, under contracts No. DE-AC02-06CH11357 (ANL), DE-FG02-94ER40834 (UMD), DE-AC02-05CH11231 (LBL), and DE-FG02-96ER40983 (UTK), the United Kingdom Science and Technology Facilities Council (STFC), and by the State of Florida.

[1] R. F. Casten, D. D. Warner, D. S. Brenner, and R. L. Gill, Phys. Rev. Lett. **47**, 1433 (1981).
[2] R. F. Casten, P. Von Brentano, K. Heyde, P. Van Isacker, and J. Jolie, Nucl. Phys. A **439**, 289 (1985).
[3] A. Faessler and W. Greiner, Z. Phys. **168**, 425 (1962).
[4] E. S. Paul *et al.*, Phys. Rev. Lett. **98**, 012501 (2007).
[5] X. Wang *et al.*, to be published.
[6] P. J. Nolan and J. F. Sharpey-Schafer, Rep. Prog. Phys. **42**, 1 (1979).
[7] N. V. Zamfir and R. F. Casten, Phys. Lett. B **260**, 265 (1991).
[8] E. S. Paul *et al.*, Phys. Rev. C **79**, 044324 (2009).
[9] I. Y. Lee, Nucl. Phys. A **520**, 641c (1990).
[10] R. V. F. Janssens and F. S. Stephens, Nucl. Phys. News **6**, 9 (1996).
[11] D. C. Radford, Nucl. Instrum. and Methods Phys. Res. A **361**, 297 (1995).
[12] D. C. Radford, M. Cromaz, and C. J. Beyer, in *Proceedings of the Nuclear Structure '98 Conference, Gatlinburg, 1998*, edited by C. Baktash (American Institute of Physics CP481, 1999), p. 570.
[13] P. Aguer, C. F. Liang, J. Libert, P. Paris, A. Peghaire, A. Charvet, R. Duffait, and G. Marguier, Nucl. Phys. A **252**, 293 (1975).
[14] C. W. Reich, Nucl. Data Sheets **99**, 753 (2003).
[15] D. R. Zolnowski, M. B. Hughes, J. Hunt, and T. T. Sugihara, Phys. Rev. C **21**, 2556 (1980).
[16] K. S. Krane, R. M. Steffen, and R. M. Wheeler, Nucl.

Data Tables A **11**, 351 (1973).
[17] T. Yamazaki, Nucl. Data A **3**, 1 (1967).
[18] A. Bohr and B. R. Mottelson, *Nuclear Structure*, Vol. II (W. A. Benjamin Inc., New York, 1975).
[19] J. Jolie, R. F. Casten, P. Cejnar, S. Heinze, E. A. McCutchan, and N. V. Zamfir, Phys. Rev. Lett. **93**, 132501 (2004).
[20] O. Scholten, F. Iachello, and A. Arima, Ann. Phys. (N.Y.) **115**, 325 (1978).
[21] F. Iachello, Phys. Rev. Lett. **85**, 3580 (2000).
[22] F. Iachello, Phys. Rev. Lett. **87**, 052502 (2001).
[23] E. A. McCutchan, N. V. Zamfir, and R. F. Casten, Phys. Rev. C **69**, 064306 (2004).
[24] J. A. Sheikh, G. H. Bhat, Y. Sun, G. B. Vakil, and R. Palit, Phys. Rev. C **77**, 034313 (2008).
[25] P. E. Garrett, J. Phys. G: Nucl. Part. Phys. **27**, R1 (2001).
[26] I. Ragnarsson and R. A. Broglia, Nucl. Phys. A **263**, 315 (1976).
[27] J. F. Sharpey-Schafer *et al.*, Nucl. Phys. A **834**, 45c (2010).
[28] J. F. Sharpey-Schafer *et al.*, Eur. Phys. J. A **47**, 5 (2011).
[29] J. F. Sharpey-Schafer, T. E. Madiba, S. P. Bvumbi, E. A. Lawrie, J. J. Lawrie, A. Minkova, S. M. Mullins, P. Papka, D. G. Roux, and J. Timar, Eur. Phys. J. A **47**, 6 (2011).
[30] Evaluated Nuclear Structure Data File, National Nuclear Data Center, Brookhaven National Laboratory, http://www.nndc.bnl.gov/ensdf (2010).
[31] A. S. Davydov and G. F. Filippov, Nucl. Phys. **8**, 237 (1958).
[32] L. Wilets and M. Jean, Phys. Rev. **102**, 788 (1956).
[33] C. Baktash, J. X. Saladin, J. J. O'Brien, and J. G. Alessi, Phys. Rev. C **18**, 131 (1978).
[34] R. F. Casten, *Nuclear Structure from a Simple Perspective* (Oxford University Press, Oxford, 1990).
[35] K. Dusling *et al.*, Phys. Rev. C **73**, 014317 (2006).
[36] G. D. Dracoulis *et al.*, Phys. Rev. C **81**, 054313 (2010).
[37] R. Bengtsson and S. Frauendorf, Nucl. Phys. A **327**, 139 (1979).
[38] S. M. Harris, Phys. Rev. Lett. **13**, 663 (1964).
[39] S. M. Harris, Phys. Rev. **138**, B509 (1965).
[40] J. Simpson, D. V. Elenkov, P. D. Forsyth, D. Howe, B. M. Nyako, M. A. Riley, J. F. Sharpey-Schafer, B. Herskind, A. Holm, and P. O. Tjom, J. Phys. G: Nucl. Phys. **12**, L67 (1986).
[41] G. D. Dracoulis, B. Fabricius, P. M. Davidson, A. O. Macchiavelli, J. Oliviera, J. Burde, F. S. Stephens, and M. A. Deleplanque, in *International Conference on Nuclear Structure at High Angular Momentum, Ottawa, 1992* (AECL-10613, 1992) Vol 2, p. 94.
[42] J. Thomson *et al.*, Phys. Rev. C **81**, 014307 (2010).
[43] K. Lagergren *et al.*, Phys. Rev. C **83**, 014313 (2011).